Straining Ge bulk and nanomembranes for optoelectronic applications: a systematic numerical analysis

Daniele Scopece[1,3], **Francesco Montalenti**[1], **Monica Bollani**[2], **Daniel Chrastina**[2] **and Emiliano Bonera**[1]

[1] Dipartimento di Scienza dei Materiali and L-NESS, Università di Milano-Bicocca, via Cozzi 53, I-20125 Milan, Italy

[2] L-NESS and Politecnico di Milano, Polo regionale di Como, via Anzani 42, I-22100 Como, Italy

E-mail: daniele.scopece.science@gmail.com and daniele.scopece@mater.unimib.it

Received 28 March 2014, revised 17 June 2014
Accepted for publication 19 June 2014
Published 5 August 2014

1. Introduction

The semiconductor technology roadmap seeks new approaches to fullfil the increasing demand for performance in electronic devices [1, 2]. This demand includes both conventional electronics and future applications in the field of optoelectronics.

In recent years strain has proven a useful tool for band engineering of Si and Ge, both as a way to increase charge carrier mobility [3] and, particularly, to modify the alignment and relative position of the bands in order to turn them into direct band gap materials [4–6]. The latter property would allow the direct integration of optoelectronics systems in current CMOS and MOSFET technology, a highly-sought after goal [7].

Germanium is an indirect-gap semiconductor, with the valence band maximum at Γ and the conduction band minimum at L. However, a local minimum exists in the conduction band at Γ which is only 140 meV above L at room temperature [8]. Tensile strain reduces this separation, and heavy n-type doping has been suggested as a way of filling up the L-valley as a possible route towards optical gain [9, 10], but with the attendant disadvantage that heavy doping leads to an increase of the optical absorption [11]. The application of 2% biaxial strain to a Ge(001) layer is expected to lower the direct gap

[3] Current address: Laboratory nanotech@surfaces, EMPA, the Swiss Federal Laboratories for Materials Science and Technology, Überlandstrasse 129, 8600 Dübendorf, Switzerland

below that of the indirect gap [12], and a similar result is expected for 4% uniaxial strain applied along [100] [13].

Although an established theory describes the effects of strain on the bands of the material [14, 15], the same effective strain can be induced by different geometries of the systems. Several solutions have been conceived to apply the desired deformation: via external stressors, cantilevers or micromachining [16–20], via particular geometry without any stressor layer [21, 22], via epitaxial growth/condensation techniques [23–25] or by the exploitation of thin nanomembranes [26, 27].

Most of the methods above apply strain to Ge micro- and nano-structures, mainly for two reasons. The first is the lack of a practical Si-based 'virtual substrate' which can be used for the direct epitaxial deposition of tensile-strained Ge layers (without introducing incompatible materials such as GeSn or InGaAs) [28, 29]. The second is that such large amounts of strain lead to very small critical thicknesses beyond which strain relaxation via onset of dislocations is energetically favored. The equilibrium critical thickness for high lattice parameter mismatch (more than 1%) can be as small as a few nanometers [30, 31], but under certain conditions (i.e. fast epitaxy at relatively low temperatures) thicker metastable films can be realized in which the nucleation of dislocations can be delayed [32, 33]. Such films can be patterned into structures which are free to relax elastically (i.e. without the introduction of dislocations), inducing strain in the substrate [34, 35].

In this configuration the strain induced in the substrate can be increased in the case that the substrate takes the form of a thin membrane rather than a thick bulk-like layer. This consideration has been presented in literature as self-evident [36], with no systematic comparison of the results in the case of massive supports versus membranes, partly due to experimental difficulties in obtaining similar conditions in the two situations. Here simulations can surely help in elucidating this issue.

In this work we systematically study some configurations of $Si_{1-x}Ge_x$ stressors and their capability to induce the necessary strain reported above in Ge substrates with a finite element method (see section 2). Our simulations aim at elucidating the role of the diverse geometric parameters of the system along with a comparison of massive, stiff Ge substrate (called 'bulk' here, section 3) with a thin, compliant one ('membrane', section 4). Our analysis tackles situations where the stressors are $Si_{1-x}Ge_x$ layers deposited epitaxially on Ge and where the geometries considered can be created with electron beam lithography. In all the results, we focus on the strain applied along [100] direction (defined 'uniaxial' here) and in the (001) plane ('biaxial'). We also systematically analyze the effect of the composition of the stressors (that can be controlled experimentally), discussing the coherency of these samples. The onset of plasticity is discussed by using known analytical formulae, since its explicit treatment is excluded from the present FEM analysis.

The understanding emerging from this study not only provides an initial guide for the experimenters in the space of the geometrical parameters, but also allows us to design a system with a very large optically active area (section 4.2) that, according to theory, seems feasible and coherent.

2. Methods

2.1. Finite-element method and work hypotheses

All the simulations are performed with a finite-element method using the commercial software Comsol Multiphysics [37], where linear elasticity theory is employed. The $Si_{1-x}Ge_x$ nanostructures are initially tetraedrically matched to the Ge lattice constant and then allowed to relax elastically. The lattice constants of $Si_{1-x}Ge_x$ alloys are based on those in [38] while the elastic constants were linearly interpolated between those of Si and Ge [39].

The accuracy of the linear elasticity theory adopted is confirmed by a number of works in literature and by previous works of the authors performed on heteroepitaxial systems as small as 10 nm wide, larger 3D islands or planar structures [40–44] leading in any case to a good agreement with experimental results. According to previous results [45], FEM can lead to discrepancies from the more accurate molecular dynamics methods in case of points inside the nanostructures or for strain higher than 7% (nonlinear effects non-negligible). Our results fall in the validity region since we focus on points outside of the nanostructures and on the strain lower than 5%.

In all simulations the directions x, y, z correspond to [100], [010] and [001] respectively. x and y are the directions in the plane and z is the normal to the free top surface. In all the simulations we apply periodic boundary conditions (PBC) in the xy plane in order to simulate and infinite bulk or membrane. This constraint imposes that the structures as a whole are not allowed to expand laterally, a condition mimicking, e.g., the anchorage of a suspended membrane to a substrate. In the simulations on bulk the bottom surface of the substrate is kept fixed, whereas in the ones on membranes it is left free to relax. Technical details of the calculations (size of the cell, mesh, etc) are reported in the supplementary material stacks.iop.org/sst/29/095012/mmedia.

2.2. Elastic strain and plastic relaxation

This work focuses on elastic strain relaxation only. In a real heterostructure, thick layers can eventually relax plastically via the nucleation of dislocations during growth. Also, the nanopatterning of a flat epilayer can lead to a significant redistribution of stress and induce plastic relaxation even in the case that the initial unstructured film was free from dislocations [46]. However, these effects depend heavily on the details of the growth and the nanofabrication. In order to provide a general analysis and general guidelines independent on the fabrication methods, in this work we do not consider in details the dynamic of nucleation of dislocations. However, we consider and highlight those structures which appear as practically feasible by comparison with metastability curves or with experimental results obtained in similar systems [35, 47].

In our simulations the interfaces are sharp. We neglect any possible intermixing effects induced to the high stress at the edges of the heteroepitaxial islands [41] in the substrate

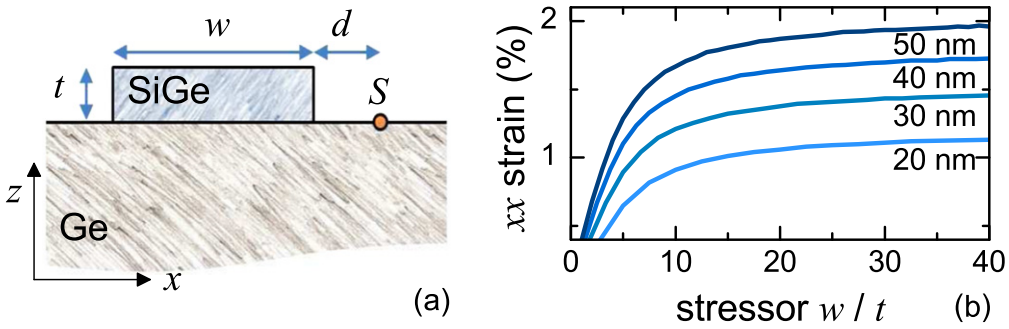

Figure 1. 'Bulk' case. (a) Sketch of the two-dimensional system. (b) Values of the ε_{xx} at point S as a function of the w/t aspect ratios for four values of t (reported under the curves) for $d = 10$ nm. See section 3.1 for details.

nearby. This effect, however, can alter the amount of strain necessary to induce a transition to a direct band gap, particularly for the cases with steep facets of the stressors close to the region of interest and should be checked in the real samples case-by-case.

3. Bulk germanium substrate

In this section we study the strain induced by $Si_{1-x}Ge_x$ nanostructures on a thick relaxed Ge substrate. The stressors are therefore tensilely stressed nanostructures of epitaxial $Si_{1-x}Ge_x$ which, by lateral shrinking, induce a tensile strain in the nearby Ge substrate via perimeter forces, whose role is discussed. In the following we will refer to the Ge layer as 'substrate', and the $Si_{1-x}Ge_x$ epilayer as 'stressor'.

Sections 3.1, 3.2 and 3.3 consider the case of a uniaxial strain, which is faster to simulate (with two-dimensional simulations) and allows the investigation of a wider range of parameters.

Section 3.4 considers the case of a biaxial strain with 3D simulations.

3.1. Uniaxial stressors: thickness and width

The geometry of the system is presented in the sketch in figure 1(a). On top of the substrate we have a lithographically-designed stripe of $Si_{1-x}Ge_x$ of width w and thickness t, infinitely extending in the y direction. In this work we are interested in engineering the strain in the substrate, and only secondarily in the strain in the stressor. Since we are interested in tensile-strained Ge, we will focus on the regions of the substrate which are not covered by the stressor, ideally able to emit light if a direct transition occurs.

The strain induced in the substrate decade with the distance from the stressors. In order to give an estimation of this strength and to reduce the large amount of data to show, we report the strain induced in a given well-defined point. In particular, we focus on the point S of figure 1(a), which is located at the surface of the Ge substrate ($z = 0$), at a distance $d = 10$ nm from the perimeter of the stressor. This choice is motivated by the fact that this is a distance which can be reached by e-beam lithography, and it is compatible with the current technological node in microelectronics.

For linear stressors, the strain at S varies as a function of the aspect ratio of the structure. This effect can be understood considering that the effect of a perimetral force can be thought of as the strain induced by two local linear forces located at the perimeter [47]. The perimeter on the right pulls S, whereas the perimeter on the left pushes away S. These point forces fade away as $1/x$, and therefore the effect of the left perimeter on S vanishes as the stressor is larger. In addition, the thicker is the stressor, the less constrained is the top surface of the structure, and therefore the elastic energy is relieved by expansion rather than transferred to the substrate [48].

Figure 1(b) analyzes the effect of the stressor geometry (aspect ratio w/t and height t) on the strain along x ([100] direction) induced on S, since we are interested in the in-plane deformation. We focus on the case of $Si_{0.50}Ge_{0.50}$ to be more realistic (in real experiments intermixing is likely to occur) and to give an estimation in the middle of the composition. Obviously a higher Si content would lead to a higher induced strain and vice versa.

Since the system is infinitely long along y direction (hidden in 2D simulations), ε_{yy} in the stressors is set from the lattice mismatch and set to zero in the Ge substrate. ε_{xy} and ε_{yz} are automatically zero both in the stressor and in the substrate. ε_{zz} and ε_{xz} in the Ge substrate are always lower than ε_{xx}, therefore their effect in altering the bands is considered negligible.

The four values of t in figure 1(b) range from 20 to 50 nm. This range of values is chosen to have a strain at S of at least 1% (for reasons to be cleared below) and to avoid irrealistically thick $Si_{1-x}Ge_x$ layers (that would likely create dislocations). As the aspect ratio increases, the strain increases because the pushing effect of the force located at the left perimeter diminishes. The plot of ε_{xx} as a function of the aspect ratio highlights that for values of w/t beyond 20, the effect of the structure on S is dominated by the right perimeter, since the strain is more than 90% of the value reached for $w/t \to \infty$. For each fixed value of w/t, thicker stressors induce higher strain. This increase is sublinear, because of the effects of the free expansion of the top surface mentioned above.

These observations have important consequences in the practical realization of the structures. First, it is important to maximize the surface ratio between strained substrate and stressor to get the highest amount of strained material on the wafer. Second, while depositing too much material is not effective in increasing the induced strain, keeping the stressor

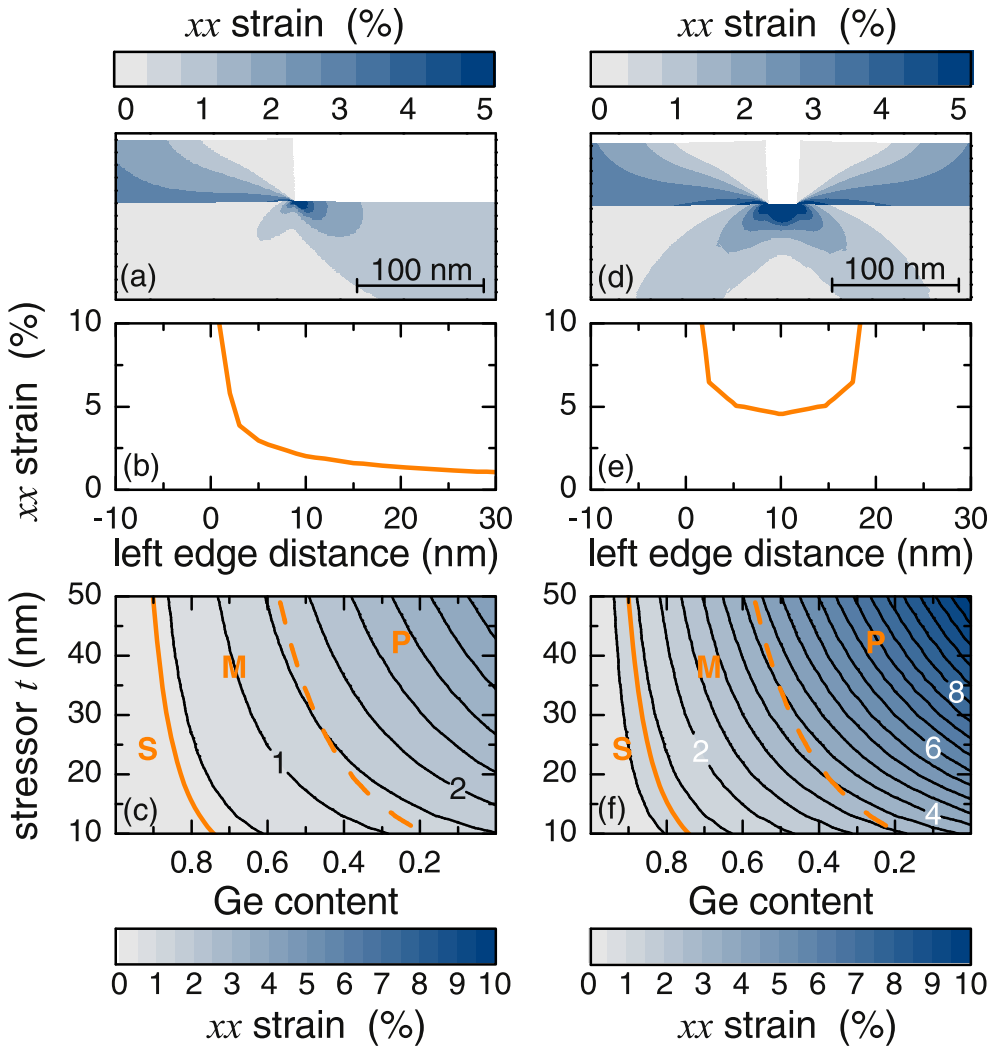

Figure 2. Uniaxial strain induced by $Si_{1-x}Ge_x$ stripes on a Ge bulk. (a) Strain values of ε_{xx} for a single $Si_{0.50}Ge_{0.50}$ stressor. (b) Values of ε_{xx} extracted from (a) at the Ge surface, close to the edge of the stressor. (c) Strain values of ε_{xx} for a single $Si_{0.50}Ge_{0.50}$ stressor at the point S (10 nm away from the stressor on the Ge surface), as a function of Ge content and the thickness of the stressor. The solid orange line represents the Matthews–Blakeslee curve for equilibrium dislocation onset. The dashed orange line represents the curve indicating the dislocation onset in metastability conditions. S, M, and P mark the stable, metastable, and plastic regions, respectively. (d)(e)(f) Same as (a) (b)(c) for two stressors. See sections 3.2 and 3.3 for details.

thin has the additional advantage of staying below the critical equilibrium or metastable thickness for relaxation [49]. Finally, a thinner stressor is easier to process by lithography and etching.

3.2. Uniaxial stressors: systematic variation with composition and height

Once established the 'infinitely-long stressor limit' in the previous section, we focus on this limit and analyze the strain distribution on other regions of Ge substrate in details and its variation with stressor composition. In case the ratio w/t of the stressors is lower than this limit, we expect the trend of ε_{xx} to follow the trend highlighted in the previous section.

Figure 2(a) reports the spatial distribution of ε_{xx} for a $Si_{0.50}Ge_{0.50}$ stressor, with $t = 50$ nm and $w = 2000$ nm (hence $w/t = 40$). This panel gives an idea of the variation of the strain with distance.

Figure 2(b) reports the values of ε_{xx} on the Ge free surface (i.e. $z = 0$) for the same calculation as a function of the distance from the edge of the stressor (hence the point S of figure 1 is at 10 nm). The decrease of ε_{xx} as a function of the distance from the perimeter is slightly softer than a $1/x$ curve, suggesting that the approximation of the linear force [47] is only partially effective. The region where the transition to the direct band condition (i.e. the active area in emission of light) is the one with $\varepsilon_{xx} > 4\%$.

Panel (c) in figure 2 resumes the results of our systematic analysis for a single stressor. It reports the values of ε_{xx} at point S (10 nm apart from the stressor edge) for different values of Ge content x in the stressors (note that higher Ge content corresponds to lower tensile strain and vice versa since here Ge is the substrate) and for different stressor thickness t. Uniaxial strain of at least 4% cannot be achieved at S, unless in the top right region of panel (c).

An important issue of these theoretical calculations is whether real stressors with this shape remain coherent or develop dislocations. This question is addressed in the same panel (c) of figure 2 by the reported curves of the critical thickness of a $Si_{1-x}Ge_x$ film on top of Ge before the onset of plastic relaxation. The solid orange curve represents the Matthews–Blakeslee limit, below which dislocations are energetically unfavourable, and therefore the system cannot present plastic relaxation [30, 49]. In addition, the dashed orange line shows a limit of metastability, derived from a similar curve taken from [50], which marks the curve below which dislocation-free film can be grown without plastic relaxation under peculiar growth-kinetic conditions, such as low temperatures and fast growth-rates. Since this limit depends strongly on the growth parameters, this curve must not be considered as a well-established sharp limit, but rather an indication that can vary significantly among different techniques.

The achievement of a high strain is therefore bound to the ability of growing an epilayer beyond this critical dimension. In this considered geometry in the region of the diagram capable of inducing a direct-gap transition ($t > 40$ nm and $x < 10\%$) the growth of a coherent film is well beyond the grasp of any known technique. An improvement is made by superposition of stressors as discussed in section 3.3.

3.3. Uniaxial stressors: strain superposition

One way to increase the strain is via superposition of the deformation fields generated by a combination of stressors. Since this is a routinely used solution, we study this possibility here giving precise values.

The simplest combination consists of two stripes of $Si_{1-x}Ge_x$ inducing tensile strain in the Ge substrate in between. Figures 2(d)–(f) are the analogous of panels (a), (b), and (c) with two stressors facing each other, with the same mesh conditions and the same substrate. Considering the point S at a distance d of 10 nm from each perimeter (the total width of the trench being 20 nm), one observes in panel (e) that ε_{xx} is about twice the corresponding case of a single stressor (as expected from the superposition of displacements).

The same conclusions can be drawn from the comparison of panels (c) and (f). It is remarkable in this case that the 4% iso-strain line (indirect-to-direct transition for uniaxial strain) overlaps with the limit of metastability, suggesting that the right combination of growth conditions might realize practically this structure in the analyzed geometry. Therefore experimental efforts towards this direction are not meaningless. This explains the reason of the choice and study of the 2% limit in the other panels and in figure 1.

These data holds for the choice of the gap performed here. Obviously (and as can be deduced from the map in panels a and d) the closer the stressors (i.e. the narrower the gap) the higher the strain induced in Ge (not shown). Here we have focused on the case of 20 nm.

3.4. Biaxial stressors

If we drop stripe stressors and consider also more complex structures, we can combine together the effect of more stressors to induce a biaxial strain, that would lead to an even better tension of the Ge substrate.

Keeping in mind the idea of the $Si_{1-x}Ge_x$ layer excavated with etching and lithographic techniques, as a representative example here we consider the case of a cross-shaped trench in a $Si_{0.50}Ge_{0.50}$ layer. Differently to the previous case, there is no free edge apart from the one between stressors to be analyzed, i.e. PBC apply to the border of the stressors also (see geometry in figure 3(a)). As compared to the uniaxial case, this is somehow equivalent to the crossing of two orthogonal trenches. In the middle of the cross the effects of four perimeter forces add up.

In order to compare with the uniaxial case, we set the arm of the cross $20/\sqrt{2}$ nm wide, so that the distance from the centre of the cross to the four corners of stressor is 10 nm, as in the previous simulation of the stripes of point S. The size of the arm of the cross is 1640 nm and the total size of the simulated wafer is 5000 nm.

Since in the middle of the cross the strain is biaxial, we need $\varepsilon_{\parallel} = 2\%$ of strain to get the indirect-to-direct transition [12], where $\varepsilon_{\parallel}$ is the in-plane strain defined as $(\varepsilon_{xx} + \varepsilon_{yy})/2$. To get this value we can relax some of the requests of the previous section. In particular, we choose to halve the previous thickness, so that $t = 20$ nm, which is still above the equilibrium limit thickness, but well below the metastability curve.

A colormap of the $\varepsilon_{\parallel}$ is reported in panels (a) and (b) of figure 3. The fact that the stress distribution is apparently non-centrosymmetric is due to the coarser mesh in the channels. In the region of interest (crossing of the channels), where the mesh is set finer, the strain field is indeed symmetric.

In this case the average biaxial strain in the crossing of the trenches is 2.06% (therefore close to the transition), with a higher value nearer the edges and a lower in the center (see figure 3(c)).

This value of strain appears to be independent of the length of the arm (a test with half a length, not shown, produces the same result) and the size of the cell (from a test with half of the cell dimension). It depends on the width of the channel only, giving higher average strain for narrower edges (2.66% for $w = 10$ nm and 1.14% for $w = 30$ nm), confirming the major role played by the edges.

The trend with the stressor composition x is expected to follow the same trend depicted in figure 2(f). For instance the case of 25% Ge in the stressor leads to a $\varepsilon_{\parallel} = 3.29\%$.

A structure like the one presented in figure 3 is technologically interesting because it can be integrated in a conventional substrate for microelectronics with legacy deposition and lithography techniques. It should be pointed out that there would be other parameters which could be changed to get the same (or higher) strain. For example, instead of reducing t one could reduce the length of the arms of the cross (which would increase the density of structures per wafer), or it would be possible to increase the width of the

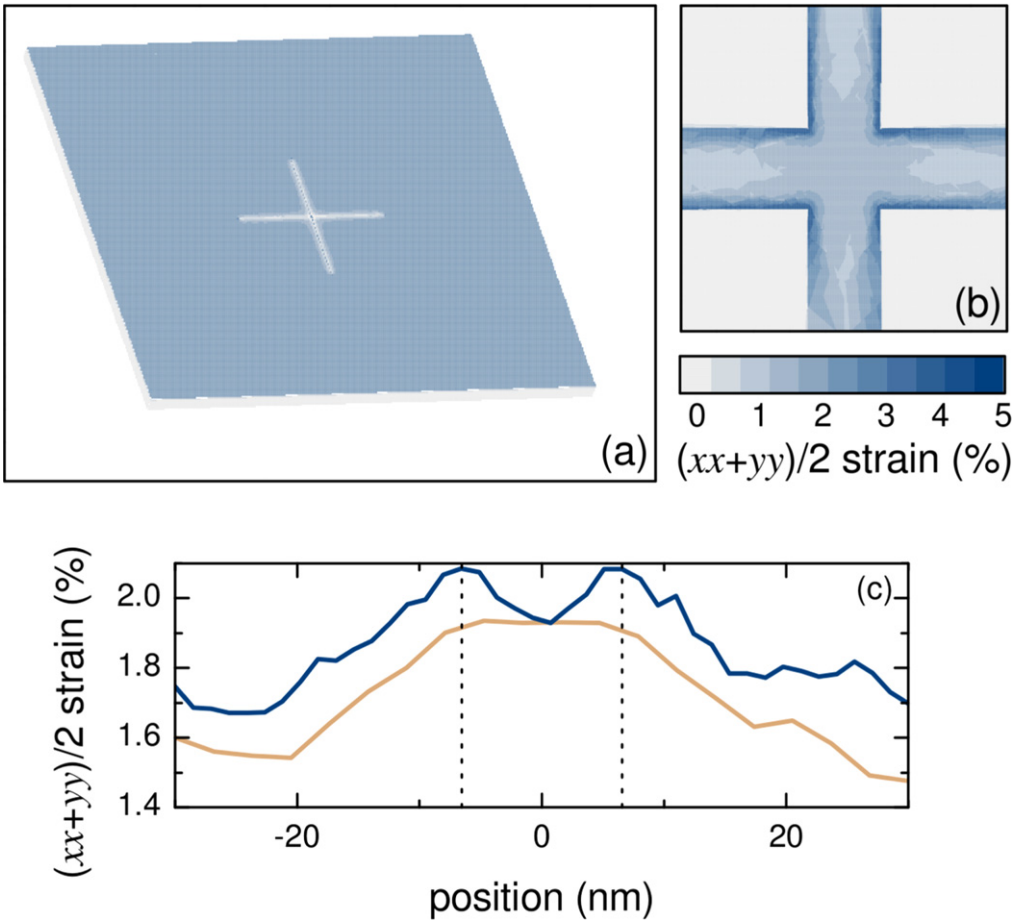

Figure 3. Biaxial stressors with the shape of two crossed trenches in $Si_{0.50}Ge_{0.50}$ on a Ge bulk substrate. The colorscale in (a,b) corresponds to the in-plane strain $(\varepsilon_{xx}+\varepsilon_{yy})/2$. (a) Tilted view of the wafer with the stressor. (b) Zoomed top view of the biaxially strained region. (c) Trend of the in-plane stress along a line at $z = 0$ (Ge surface) parallel to x axis passing in the middle of the active area ($y = 0$, red, lower curve) and at 1/4 of its length ($y = 3$ nm, blue, upper curve). In (c) the vertical black lines delimitate the region of the active area, where the mesh is built finer and the field is symmetric with respect to the center of the zone ($x = y = z = 0$). See section 3.4 for details.

arms (which would broaden the active area of each single structure), with the *caveat* that larger arms would generically lead to a lowering of the strain induced, given the larger distance of the center of the active area from the edges of the stressors. One last possibility could be to couple the biaxial region of direct bandgap with other regions of unixial strain along the arms of the cross, provided they can be made narrower or the stressors thicker in order to reach the 4% limit needed. This would increase the density of the active area considerably on the wafer.

4. Germanium membranes

The previous results hold for an infinitely thick substrate, supposed rigid. As stated in the introduction, in literature the trend is to consider thin membranes that can be deposited on different substrates, or a standing membrane obtained by excavating a bulk.

In this section we analyze this case. In the simulations the free standing membrane translates into a bottom surface of the substrate free to relieve strain by bending. An infinitely long membrane is studied by applying (as in the case of a 'bulk') periodic boundary conditions in the plane of the membrane. In these cases the thickness t_{Ge} of the substrate is taken comparable to the one of the stressors t, since this is what occurs experimentally.

4.1. Uniaxial stressors and the onset of a maximum

In order to understand the stress field in these geometries, figure 4(a) reports a representative example of the entire cell in the deformed state. As in the previous uniaxial figures here the stressors are $Si_{0.50}Ge_{0.50}$ atop of a pure Ge membrane, but in this case the only termination of the stressors is the gap between them (set to 20 nm, as before). This configuration is chosen in order to focus the effect of the stress and of the bending on a single cavity. Additional terminations of the stressors would affect the entire bending and stress field so as to make the analysis difficult. This configuration makes the effective length of the stressors (considering the replication with PBC) equal to 1000 nm. Both the stressors and the Ge membrane are 50 nm thick. The bending caused by the tensile effect of the stressors is evident.

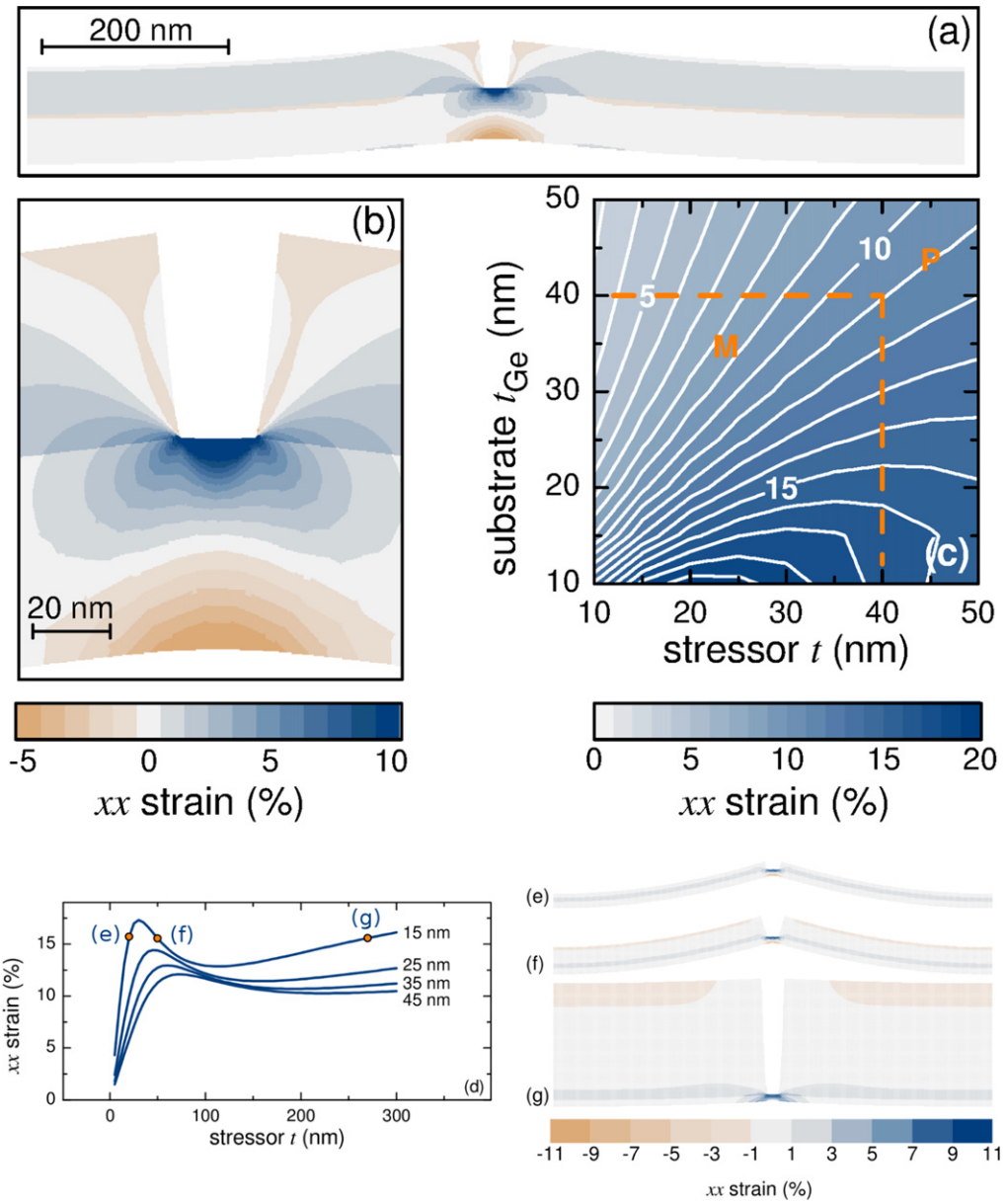

Figure 4. (a,b) $Si_{0.50}Ge_{0.50}$ stressors with thickness of 50 nm on top of a Ge membrane of 50 nm. The spacing in between the stressor arms is 20 nm. The color scale is reported below panel (b). (c) Map of ε_{xx} strain in the point S (in the middle of the gap) for $Si_{0.50}Ge_{0.50}$ stripes as stressor of a Ge membrane. The meaning of the dashed line, M and P are the same as in figure 2. (d) Trend of ε_{xx} along horizontal lines in (c) to show the maximum for different t_{Ge}(different curves) and for larger t. (e,f,g) deformation plots of the points highlighted in (d). See section 4.1 for details and discussion.

The colormap is the strain ε_{xx}. Its colorbar is located under panel (b), an enlargement in the region of the gap. In this configuration the strain ε_{xx} computed in the middle of the gap (point S discussed above) is 10.6%. If on one side this value is for sure higher than the 4% required to have a transition to direct band gap, on the other it is not clear how the bands would look like with such a high strain [14] and the validity of the linear elasticity theory itself is doubtful [45].

The reason for this increase of strain towards the Ge side with respect to the results the Ge bulk reported in figure 2 is twofold. First, the elastic energy can now be almost equally shared by the stressors and the membrane, leading to a higher deformation of the membrane. Second, a geometrical effect arises from the fact that the SiGe/Ge regions curl upwards following the behavior described by the Stoney/Timoshenko theory for strained bilayers [51]. The large upward-curled regions exert strong forces on the small regions in the stressor trench where S is positioned. The resulting downward curling of the trench region creates a high positive strain on the top surface of Ge, and a high negative strain in the bottom surface of Ge.

One important issue is the dependence of the strain induced by the bending with different total length of the stressors, given this chosen geometry, since intuitively the bending will be different for a different length of the membrane/stressors. Indeed in this case, contrary to the case of

section 3.4, there is no stiff bulk to fix the relaxation. Additional simulations with different length of substrate and stressors with the same geometry (not reported) show that there is not any infinite-long limit, but rather the strain induced in the gap increases with the length of the membrane. Simulations with stressor length equal to 250 nm (500 nm in the repeated cell), 500 nm (shown in figure 4(a)), 750 nm and 1000 nm report a value of ε_{xx} equal to 7.21%, 10.67%, 12.72% and 14.07%, respectively.

As in the case of bulk-like structure, the height of the stressor are influencing the relaxation. Differently from that case, however, here it is also the height of the membrane that plays a role.

Figure 4(c) reports the isolines of the ε_{xx} at point S in the middle of the channel when the values of t and t_{Ge} are lower than 50 nm. The sample width is kept fixed to the one reported in panel (a). Here the regions of metastability (M) and plasticity (P) are highlighted.

The limiting situations of $t/t_{Ge} \ll 1$ and $t/t_{Ge} \gg 1$ can be considered as analogs of the bulk case (where the bulk is Ge or $Si_{1-x}Ge_x$, respectively). The first difference with the case of the bulk substrate is that while the isostrain curves of figure 2(a) are always monotonic with t, figure 4(c) shows also a strain maximum for conditions close to t = 30 nm and t_{Ge} = 20 nm.

An example of this non-monotonicity is reported in figure 4(d) for four different values of t_{Ge} (horizontal lines in panel c) and for larger values of t. The deformed plots of points (e), (f) and (g) are reported in the panels with the same name.

The maximum occurs at a condition close to the $t = t_{Ge}$, where it is most energetically favourable to distort both the membrane and the stressor. A thicker membrane (or a thicker stressor) limits this deformation and hence strain accumulation.

One issue to address is the dependence of the occurrence of this maximum with the length of the cells, since the elastic response is different. A second simulation with the stressor length equal to 1000 nm (2000 nm in the repeated cell, not reported) is compared with this result (500 nm of the length of the stressor). In the case of longer cell and stressor a higher strain is achieved: at the maximum for t_{Ge} = 15 nm a value of 27% is reached as compared to 17%. Additionally the maximum occurs at a higher value of t (at ≈39 nm vs ≈30 nm for the shorter case). But the trend of the curve is unaltered, showing also the monotonic, asymptotic increase for large values of t (t > 100 nm).

This phenomenon leads to the unique situation that a high strain is registered for thin stressors and membrane, contrary to the case of the bulk. These results thoroughly support the idea that a compliant substrate can be used to increase the strain considerably provided a tuning of the geometrical parameters is considered, as currently performed in literature.

4.2. Biaxial stressors

To complete our analysis and the comparison with the bulk-like substrate, here we investigate the generation of biaxial strain in a Ge membrane with the same geometry as in figure 3. As in the previous section, in order to create a membrane, in this case the Ge substrate is reduced to a size comparable to the stressor and its bottom surface made free to relax.

Considering the results in figure 4(c), we choose to set $t = t_{Ge}$ = 20 nm, since they induce a high strain but are thick enough to be feasible experimentally. As in section 3.4, the size of the arm of the cross is 1640 nm, the total dimension of the simulated membrane is 5000 nm, the stressor is $Si_{0.50}Ge_{0.50}$ and PBC are applied in the plane xy.

Because of the high strain induced in the structure by the reduction of the substrate thickness and by its compliancy, the goal of $\varepsilon_{\|}$ = 2% can be achieved with much more relaxed design values as compared to figure 3. In this example, we increase considerably the width of the cross arms to 400 nm, more than one order of magnitude larger than the bulk case.

As in the uniaxial case, figure 5(a) shows an upward curling of the membrane in correspondence of the arms of the cross, with a downward curling in correspondence of the centre of the cross. With these values, $\varepsilon_{\|}$ is still considerably larger than 2% in the whole region within the centre of the cross (about 2.67%). This example represents a case of a very large area optically active (≈400 × 400 nm^2, considering that the value given is an average one on this area).

The trend of the $\varepsilon_{\|}$ along a line crossing the center of the channel at $y = z = 0$ is reported in figure 5(c) along with the line at y = 100 nm (located at 1/4 of the trench width). Highly homogeneous values in the entire active region are registered.

The value of strain increases if the width of the cross is decreased. For a w equal to 200 nm or 100 nm the strain increases to 4.50% and 6.60%, respectively. By increasing the thickness of both the membrane and the stressor to 30 nm the strain just slightly decreases (2.63%). By halving the lateral size of the system to 2500 nm, the strain just slightly decreases to 2.13%. By decreasing the Ge content in the stressor to 25% the in-plane strain increases to 4.15%.

As in section 3.4, also in this case we could have relaxed other parameters to get a similar $\varepsilon_{\|}$, such as a thicker membrane, or a shorter cross-arm, or even a different shape. The result reported here demonstrates nevertheless that, as compared to bulk, there is much room for achievement of large areas of highly strained Ge if a membrane is employed.

5. Conclusions

In this paper, we investigated the strain induced by $Si_{1-x}Ge_x$ stressors on Ge substrates with the aim to understand the optimal geometrical and compositional configurations to induce elastically high tensile strain in Ge substrates.

The goal is indeed to tune the functional properties of Ge to transform it into a direct-band material suitable for optoelectronics applications. We discussed the strain in the

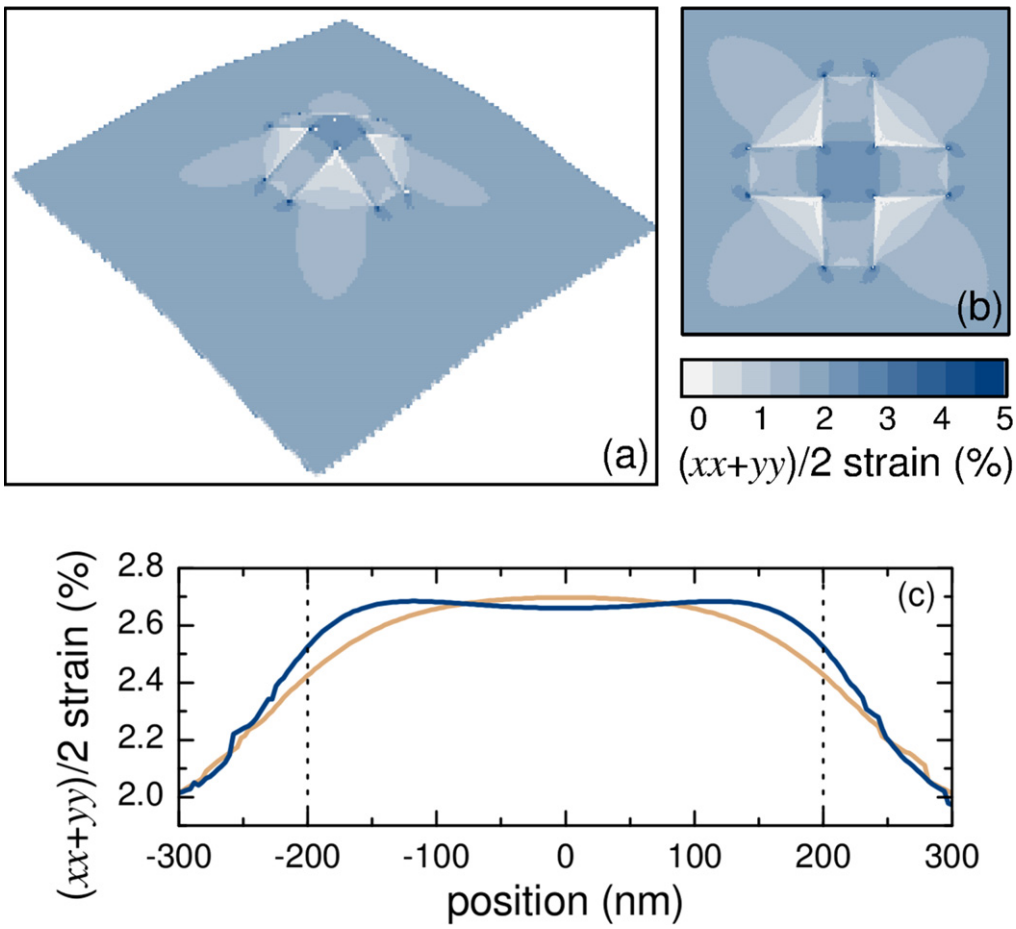

Figure 5. $Si_{0.50}Ge_{0.50}$ biaxial stressors with the shape of two crossed trenches on a Ge membrane. The width of the trenches is 400 nm. The colorscale maps the in-plane strain ($\varepsilon_{xx}+\varepsilon_{yy}$)/2. (a) Tilted view of the membrane with the stressor. (b) Zoomed top view of the biaxially strained region. (c) In-plane strain on the Ge surface ($z = 0$) along lines parallel to [100] direction passing through the center of the trenches ($y = 0$ nm, red curve) and at 1/4 of its width ($y = 100$ nm, blue curve). The dashed lines delimitate the region where the trenches cross, where the mesh is finer. See section 4.2 for details.

heterostructures in terms of contributions from strain sharing, perimetral forces and geometrical effects.

By focusing on the elastic properties of stressors feasible with lithographic techniques and on the threshold value of both uniaxial and biaxial strain to create a direct band gap material, we highlighted the existence of an infinitely-long limit of stressors, the effect of the stressors composition, the utility of deformation superposition due to more than one stressor and a biaxial configuration.

We reported a quantitative and systematic estimation of the enhancement of strain moving from a bulk substrate towards a compliant thin membrane, providing a qualitative physical insight behind the improvement guaranteed by the latter. Our analysis on compliant membranes has highlighted the onset of a maximum for thin stressors and substrates that could be exploited in future devices. The 3D case of the compliant substrate has shown a possibility to have a large optically active area, important feature to allow the integration on CMOS technology.

For these reasons, this paper can provide guidelines for designing top-down nanostructures for intense strain engineering of germanium.

It would be interesting for the community the identification and measurement of real samples with such characteristics. These will be performed in future publications on selected cases.

Acknowledgments

This work was supported by Fondazione Cariplo, grant DefCon4 2011–0331. DS kindly acknowledges Francesca Boioli for her support in plotting the strain maps.

References

[1] Thompson S E, Sun G Y, Choi Y S and Nishida T 2006 Uniaxial-process-induced strained-si: extending the cmos roadmap *IEEE Trans. Electron Devices* **53** 1010–20
[2] Miller D A B 2009 Device requirements for optical interconnects to silicon chips *Proc. IEEE* **97** 1166–85
[3] Whall T E and Parker E H C 1998 Sige heterostructures for FET applications *J. Phys. D: Appl. Phys* **13** 1397

[4] Kurdi M E, Fishman G, Sauvage S and Boucaud P 2010 Band structure and optical gain of tensile-strained germanium based on a 30 band k·p formalism *J. Appl. Phys.* **107** 013710

[5] Pizzi G, Virgilio M and Grosso G 2010 Tight binding calculation of optical gain in tensile strained [001]-Ge/SiGe quantum wells *Nanotechnology* **21** 055202

[6] Sun X, Liu J, Kimerling L C and Michel J 2010 Toward a germanium laser for integrated silicon photonics *IEEE J. Sel. Top. Quantum* **16** 124–31

[7] Soref R 2010 Mid-infrared photonics in silicon and germanium *Nat. Photonics* **4** 495–7

[8] Madelung 1982 *Landolt–Börnstein: Numerical Data and Functional Relationships in Science and Technology* 3rd edn vol 17a (New York: Springer) pp 3–4 chapter 2, 19–22, 43–68, 87–110 excerpts from band data of Si and Ge, explanation of the used abbrev.

[9] Liu J, Sun X, Pan D, Wang X, Kimerling L C, Koch T L and Michel J 2007 Tensile-strained, n-type Ge as a gain medium for monolithic laser integration on Si *Opt. Express* **15** 11272–7

[10] Camacho-Aguilera R E, Cai Y, Patel N, Bessette J T, Romagnoli M, Kimerling L C and Michel J 2012 An electrically pumped germanium laser *Opt. Express* **20** 11316–20

[11] Carroll L, Friedli P, Neuenschwander S, Sigg H, Cecchi S, Isa F, Chrastina D, Isella G, Fedoryshyn Y and Faist J 2012 Direct-gap gain and optical absorption in germanium correlated to the density of photoexcited carriers, doping, and strain *Phys. Rev. Lett.* **109** 057402

[12] Vogl P, Rieger M M, Majewski J A and Abstreiter G 1993 How to convert group-IV semiconductors into light emitters *Phys. Scr.* **T49B** 476–82

[13] Aldaghri O, Ikonić Z and Kelsall R W 2012 Optimum strain configurations for carrier injection in near infrared Ge lasers *J. Appl. Phys.* **111** 053106

[14] Fischetti M V and Laux S E 1996 Band structure deformation potentials and carrier mobility in strained Si Ge and SiGe alloys *J. Appl. Phys.* **80** 2234–52

[15] Tahini H, Chroneos A, Grimes R W, Schwingenschloegl U and Dimoulas A 2012 Strain-induced changes to the electronic structure of germanium *J. Phys.: Condens. Matter* **24** 195802

[16] Lim P H, Park S, Ishikawa Y and Wada K 2009 Enhanced direct bandgap emission in germanium by micromechanical strain engineering *Opt. Express* **17** 16358–65

[17] Ghrib A, de Kersauson M, Kurdi M E, Jakomin R, Beaudoin G, Sauvage S, Fishman G, Ndong G, Chaigneau M, Ossikovski R, Sagnes I and Boucaud P 2012 Control of tensile strain in germanium waveguides through silicon nitride layers *Appl. Phys. Lett.* **100** 201104

[18] Greil J, Lugstein A, Zeiner C, Strasser G and Bertagnolli E 2012 Tuning the electro-optical properties of germanium nanowires by tensile strain *Nano Lett.* **12** 6230–4

[19] Jain J R, Hryciw A, Baer T M, Miller D A B, Brongersma Mark L and Howe R T 2012 A micromachining-based technology for enhancing germanium light emission via tensile strain *Nat. Photonics* **6** 398–405

[20] Capellini G *et al* 2013 Strain analysis in sin/ge microstructures obtained via si-complementary metal oxide semiconductor compatible approach *J. Appl. Phys.* **113** 013513

[21] Minamisawa R A, Spolenak M J, Faist J, David C, Gobrecht J, Bourdelle K K and Sigg H 2012 Top-down fabricated silicon nanowires under tensile elastic strain up to 4.5% *Nat. Commun.* **3** 1096

[22] Süess M J, Geiger R, Minamisawa R A, Schiefler G, Frigerio J, Chrastina D, Isella G, Spolenak R, Faist J and Sigg H 2013 Analysis of enhanced light emission from highly strained germanium microbridges *Nat. Photonics* **7** 466–72

[23] Oda K, Okumura T, Tani K, Saito S i and Ido T 2012 Improvement of photoluminescence from Ge layers with Si_3N_4/SiO_2 stressors *IEEE 9th Int. Conf. Group IV Photonics* 334–6

[24] Huang S, Lu W, Li C, Huang W, Lai H and Chen S 2012 A CMOS-compatible approach to fabricate an ultra-thin germanium-on-insulator with large tensile strain for Si-based light emission *Opt. Express* **21** 640–6

[25] Tani K, Saito S i, Oda K, Okumura T, Mine T and Ido T 2012 Lateral carrier injection to germanium for monolithic light sources *IEEE 9th Int. Conf. Group IV Photonics* 328–30

[26] Boztug C, Sánchez-Pérez J R, Sudradjat F F, Jacobson R B, Paskiewicz D M, Lagally M G and Paiella R 2012 Tensilely strained germanium nanomembranes as infrared optical gain media *Small* **8** 357–61

[27] Roberts M M, Klein L J, Savage D E, Slinker K A, Friesen M, Celler G, Eriksson M A, Lagally M A X G and Drive C 2006 Elastically relaxed free-standing strained-silicon nanomembranes *Nat. Mater.* **5** 388

[28] Soref R, Kouvetakis J, Tolle J, Menendez J and D'Costa V 2007 Advances in SiGeSn technology *J. Mater. Res.* **22** 3281–91

[29] Huo Y, Lin H, Chen R, Makarova M, Rong Y, Li M, Kamins T I, Vuckovic J and Harris J S 2011 Strong enhancement of direct transition photoluminescence with highly tensile-strained Ge grown by molecular beam epitaxy *Appl. Phys. Lett.* **98** 011111

[30] Matthews J W and Blakeslee A E 1974 Defects in epitaxial multilayers–I. Misfit dislocations *J. Cryst. Growth* **27** 118–25

[31] Matthews J W 1975 Defects associated with the accommodation of misfit between crystals *J. Vac. Sci. Technol.* **12** 126–33

[32] People R and Bean J C 1985 Calculation of critical layer thickness versus lattice mismatch for Ge_xSi_{1-x}/Si strained-layer heterostructures *Appl. Phys. Lett.* **47** 322–4

[33] Beanland R 1992 Multiplication of misfit dislocations in epitaxial layers *J. Appl. Phys.* **72** 4031–5

[34] Chrastina D, Vanacore G M, Bollani M, Boye P, Schöder S, Burghammer M, Sordan R, Isella G, Zani M and Tagliaferri A 2012 Patterning-induced strain relief in single lithographic SiGe nanostructures studied by nanobeam x-ray diffraction *Nanotechnology* **23** 155702

[35] Bollani M, Chrastina D, Fiocco M, Mondiali V, Frigerio J, Gagliano L and Bonera E 2012 Lithographically-defined low dimensional SiGe nanostripes as silicon stressors *J. Appl. Phys.* **112** 094318

[36] Opotowsky A C, Scott S A, Ritz C S, Savage D E, Celler G K and Lagally M G 2007 Structure of elastically strain-sharing silicon(110) nanomembranes *New J. Phys.* **9** 270

[37] COMSOL Inc. COMSOL Multiphysics User's Guide manual. 2012

[38] Dismukes J P, Ekstrom L and Paff R J 1964 Lattice parameter and density in germanium-silicon alloys *J. Phys. Chem.* **68** 3021–7

[39] Wortman J J and Evans R A 1965 Young's modulus, shear modulus, and Poisson's ratio in silicon and germanium *J. Appl. Phys.* **36** 153–6

[40] Chen G, Sanduijav B, Matei D, Springholz G, Scopece D, Beck M J, Montalenti F and Miglio L 2012 Formation of Ge nanoripples on vicinal Si (1 1 10): from Stranski-Krastanow seeds to a perfectly faceted wetting layer *Phys. Rev. Lett.* **108** 055503

[41] Zhang J J *et al* 2010 Collective shape oscillations of SiGe islands on pit-patterned Si(001) substrates: a coherent-growth strategy enabled by self-regulated intermixing *Phys. Rev. Lett.* **105** 166102

[42] Sanduijav B, Scopece D, Matei D, Schaffler F, Miglio L and Springholz G 2012 One-dimensional to three-dimensional ripple-to-dome transition for sige on vicinal si(1 1 10) *Phys. Rev. Lett.* **109** 025505
[43] Montalenti F, Scopece D and Miglio L 2013 Comptes rendus physique dominant role of surface energy *C. R. Phys.* **14** 542–52
[44] Zhang J J, Rastelli A, Schmidt O G, Scopece D, Miglio L and Montalenti F 2013 Self-organized evolution of Ge/Si(001) into intersecting bundles of horizontal nanowires during annealing *Appl. Phys. Lett.* **103** 083109
[45] Pryor C, Kim J, Wang L W, Williamson A J and Zunger A 1998 Comparing of two methods for describing the strain profiles in quantum dots *J. Appl. Phys.* **83** 2548
[46] Hu S M 1991 Stress-related problems in silicon technology *J. Appl. Phys.* **70** 53–80
[47] Bonera E, Bollani M, Chrastina D, Pezzoli F, Picco A, Schmidt O G and Terziotti D 2013 Substrate strain manipulation by nanostructure perimeter forces *J. Appl. Phys.* **113** 164308
[48] Miglio L and Montalenti F 2011 (*Silicon-Germanium (SiGe) Nanostructures: Production, Properties, and Applications in Electronics*) ed Y Shiraki and N Usami (Cambridge: Woodhead Publishing Limited) (chapter 10)
[49] Shiraki Y and Sakai A 2005 Fabrication technology of sige hetero-structures and their properties *Surf. Sci. Rep.* **59** 153
[50] Paul D J 2004 Si/sige heterostructures: from material and physics to devices and circuits *Semicond. Sci. Technol.* **19** R75
[51] Timoshenko S 1925 Analysis of bi-metal thermostats *J. Opt. Soc. Am.* **11** 233